Observation of Rabi-oscillation-driven cyclical noise squeezing in active quantum dot ensembles

Ori Gabai,[1,*] Amnon Willinger,[1,*] Igor Khanonkin,[1,*] Vitalii Sichkovskyi,[2] Johann Peter Reithmaier,[2] and Gadi Eisenstein[1,†]

[1]*Faculty of Electrical and Computer Engineering and the Helen Diller Quantum Center, Technion—Israel Institute of Technology, Haifa, Israel*

[2]*Institute of Nanostructure Technologies and Analytics, Technische Physik, CINSaT, Kassel University, Kassel, Germany*

(Received 8 May 2026; accepted 14 October 2026; published 5 November 2026)

Squeezed light is usually generated using parametric processes in various nonlinear materials. Semiconductor lasers and optical amplifiers (SOAs) also offer nonlinearities, but they differ in that they add amplified spontaneous emission originating from population inversion, which represents a thermal state. Squeezing to below the vacuum level has been demonstrated in a semiconductor laser, and gain saturation in SOAs can likewise reduce field amplitude fluctuations to below the vacuum limit. Here, we demonstrate that Rabi oscillations in room-temperature quantum dot SOAs induced by short resonant pulses cause cyclical noise modification that repeats with every change of 2π in pulse area. Homodyne measurements reveal in those cases elliptical Wigner functions corresponding to displaced squeezed thermal states and in some cases those corresponding to squeezing below the vacuum level. At other pulse areas, the Wigner functions are circular representing displaced thermal states. This periodic behavior persists over two orders of magnitude in input pulse energy. Under specific bias and excitation conditions, we further observe a non-Gaussian Wigner function featuring two bright lobes. Such a Wigner function does not represent any known quantum state. It resembles though a Schrödinger catlike non-Gaussian state, and we speculate that the accompanying negativity is suppressed due to an approximately 10 dB optical output loss. This speculation is confirmed by a simulation. Notably, the emergence of this non-Gaussian state is itself periodic in excitation pulse energy.

DOI: 10.1103/7qbs-778n

I. INTRODUCTION

Squeezed light is a nonclassical state of an optical signal in which the uncertainty in one quadrature (e.g., the field amplitude) is reduced at the expense of the other quadrature (the phase), while obeying the Heisenberg uncertainty [1–3]. Squeezed optical signals allow for improved quantum sensing, computation, and communication [4–9]. Generation of squeezed light requires a strong nonlinearity, which is most often implemented in $\chi^{(2)}$ or $\chi^{(3)}$ materials [10–14].

Strong nonlinearities are also available in optically active semiconductor devices such as lasers and optical amplifiers. Such optically active media differ from passive materials in that they add amplified spontaneous emission (ASE) noise. The nonlinearity in an active device, and its consequent ability to squeeze the noise, stems from saturation, which is determined, in turn, by the medium dynamical properties. The dynamics of semiconductor devices are fast, and this has a major impact on the noise properties under saturated conditions [15–17].

Squeezing in a dc driven semiconductor laser was demonstrated by Y. Yamamoto's group several decades ago [18,19]. Similar squeezing levels were achieved in A. Yariv's group by applying a weak dispersive feedback to the laser [20]. A recent paper [21] reported squeezing in a quantum dot (QD) laser driven by an ultralow-noise current source. A model for squeezing in semiconductor lasers was described in Ref. [22]. The noise of a saturated semiconductor laser and optical amplifier (SOA) was shown both theoretically and experimentally to exhibit a spectral hole in the spectral vicinity of the saturating signal [15,23,24]. Clear narrowing of the statistical distribution of the power spectral density in a saturated SOA was demonstrated experimentally for continuous waves (CWs) [25] as well as pulse [26] excitations, and confirmed by a simulation [27].

Ultrashort pulse propagation in an SOA induces several nonlinear coherent interactions [28]. Once the pulses are sufficiently intense and their duration is short in comparison to the semiconductor coherence time (which is roughly 1 ps at room temperature [29]), they induce coherent interactions such as Rabi oscillations, which were demonstrated experimentally mainly in QD SOAs [28,30–32], but also in a quantum cascade laser [33], and were modeled for quantum well SOAs [34]. This means that as the pulse propagates, the SOA oscillates between gain and absorption on the timescale of the pulse. This leaves a direct imprint on the temporal profiles of the amplitude and phase of the SOA output pulse. The carrier density in the SOA also oscillates and this affects

*These authors contributed equally to this work.
†Contact author: gad@technion.ac.il

Published by the American Physical Society under the terms of the Creative Commons Attribution 4.0 International license. Further distribution of this work must maintain attribution to the author(s) and the published article's title, journal citation, and DOI.

the amplified spontaneous emission noise accompanying the pulse.

We demonstrate here, a direct interplay between Rabi oscillations and noise in a QD SOA operating at 1550 nm and at room temperature. To induce Rabi oscillations, we excite the QD SOA with resonant 100 fs pulses and characterize the noise of the resulting output pulses using homodyne detection, where a replica of the excitation pulse acts as the local oscillator (LO). During the portions of the Rabi cycle when the quantum dots provide gain, the uncertainty in the field amplitude is reduced, yielding an elliptical Wigner function. The Wigner function is a common graphical representation describing quantum states. It is obtained by a mathematical analysis of the output of a homodyne measurement. Negative regions in the Wigner function represent a true quantum state that cannot be described by any classical probability distribution [35]. We highlight two key results. First, the noise modification is cyclical with the input pulse excitation energy repeating with every fourfold increase of the pulse energy, which amounts to a 2π increase in pulse area, namely, a full cycle on the Bloch sphere. This periodic behavior extends over a very wide range of excitation pulse energies, from 1.58 to 158 pJ. Some of these elliptical Wigner functions represent states that are squeezed to below the vacuum level, and others describe displaced squeezed thermal states [36]. The latter are elliptical Wigner functions that are placed away from the origin, where the variance of one quadrature is equal to or smaller than that of the thermal state. Other pulse areas yield circular or slightly elliptical Wigner functions describing displaced thermal states [37] resulting from the addition of the SOA's ASE.

Second, in some cases, the obtained Wigner function is non-Gaussian comprising two separated bright lobes. Such a Wigner function does not represent any known quantum state. We speculate that it describes a Schrödinger catlike non-Gaussian state where the corresponding negativity is not observable due to a 10 dB output optical loss as predicted in Ref. [38]. There are various contributions to the total loss budget. Input coupling and collection to and from the amplifier amount to 6.5 dB, which were carefully measured. Measured propagation losses through the optical system including spectral filtering add 1.5 dB. The detector efficiency stated by the manufacturer (in units of A/W) and confirmed by measurements is 0.95 (−0.25 dB) at a wavelength of 1550 nm, corresponding to a calculated photodetection quantum efficiency of approximately 76%. The imperfect overlap between the interfering beams can only be estimated. It is assumed to be roughly 0.6, which adds another 2.25 dB. The total loss is therefore 10.5 dB, but since there are slight uncertainties we consider this as an upper limit and use 10 dB as the total loss of the optical system.

Finally, the observation of this non-Gaussian state is also cyclical, recurring with a 2π increase in pulse area.

II. RESULTS

A. Observation of cyclical noise squeezing

The experimental setup for homodyne characterization of ultrashort pulses following coherent interaction with a room-temperature QD SOA is shown in Fig. 1. A 100 fs laser pulse is split with one part serving as the LO, while the second is coupled to a QD optical amplifier. The QD SOA comprises six layers of high-density, 6×10^{10} cm^{-2}, InAs QDs grown by molecular beam epitaxy in the Stranski-Krastanow mode. The optical amplifier was fabricated as a 2 μm wide, 1.5 mm long ridge waveguide whose end facets were antireflection coated. Further details of the device fabrication and characterization are given in Ref. [39]. The amplifier was operated with a dc bias of 7 kA/cm^2. This bias level is roughly three times higher than the original device threshold [before antireflection (AR) coating] and provides a gain of 20 dB. The gain dictates the effective dipole moment and together with the excitation pulse electrical field intensity determines the Rabi frequency and hence nature of the cyclical gain and noise squeezing.

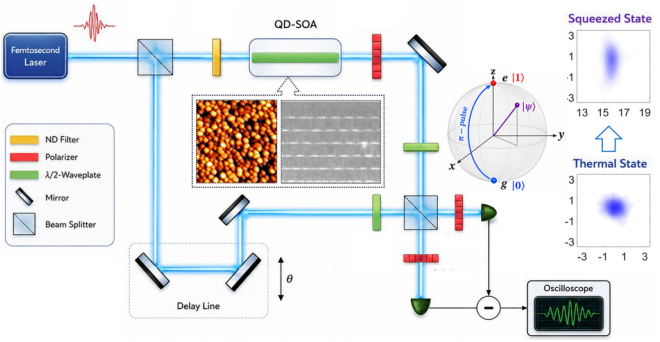


FIG. 1. Experimental setup for homodyne detection of femtosecond pulses following the interaction with a QD ensemble. The two small insets show exemplary Wigner functions of a thermal state (stemming from the spontaneous emission noise) and of a squeezed state.

The LO is shot noise limited as shown in Appendix A. Following the interaction with the QD SOA, the transmitted field (signal) is recombined with the LO, whose relative phase is controlled via an optical delay line. The resulting interference is detected by a balanced photodetector, and the difference signal is recorded using an oscilloscope.

Scanning the LO phase over 2π radians for about one thousand times yields a histogram of the current uncertainty. The histogram is transformed into a Wigner function using the inverse Radon transform [40]. This transform is intended for CW or narrow-spectrum signal. The spectral width of the 100 fs excitation pulses is roughly 3% of the optical frequency, and hence, the assumption of a narrow band signal is valid. The insets in Fig. 1 show, respectively, the Wigner functions of the ASE noise under linear conditions, namely, with no input signal, and of a typical squeezed state.

The homodyne system serves also as a cross-correlator where the LO pulse samples the signal pulses after propagating through the QD gain medium while the relative temporal delay between them is scanned. Such cross-correlations for three different excitation pulse energies are shown in the left column of Fig. 2. The cross-correlations reveal that the 100 fs excitation pulse broadens to about 1 ps and attains an amplitude profile resembling the results measured using cross-correlation frequency-resolved optical gating [30]. Homodyne measurements were performed with the LO sampling

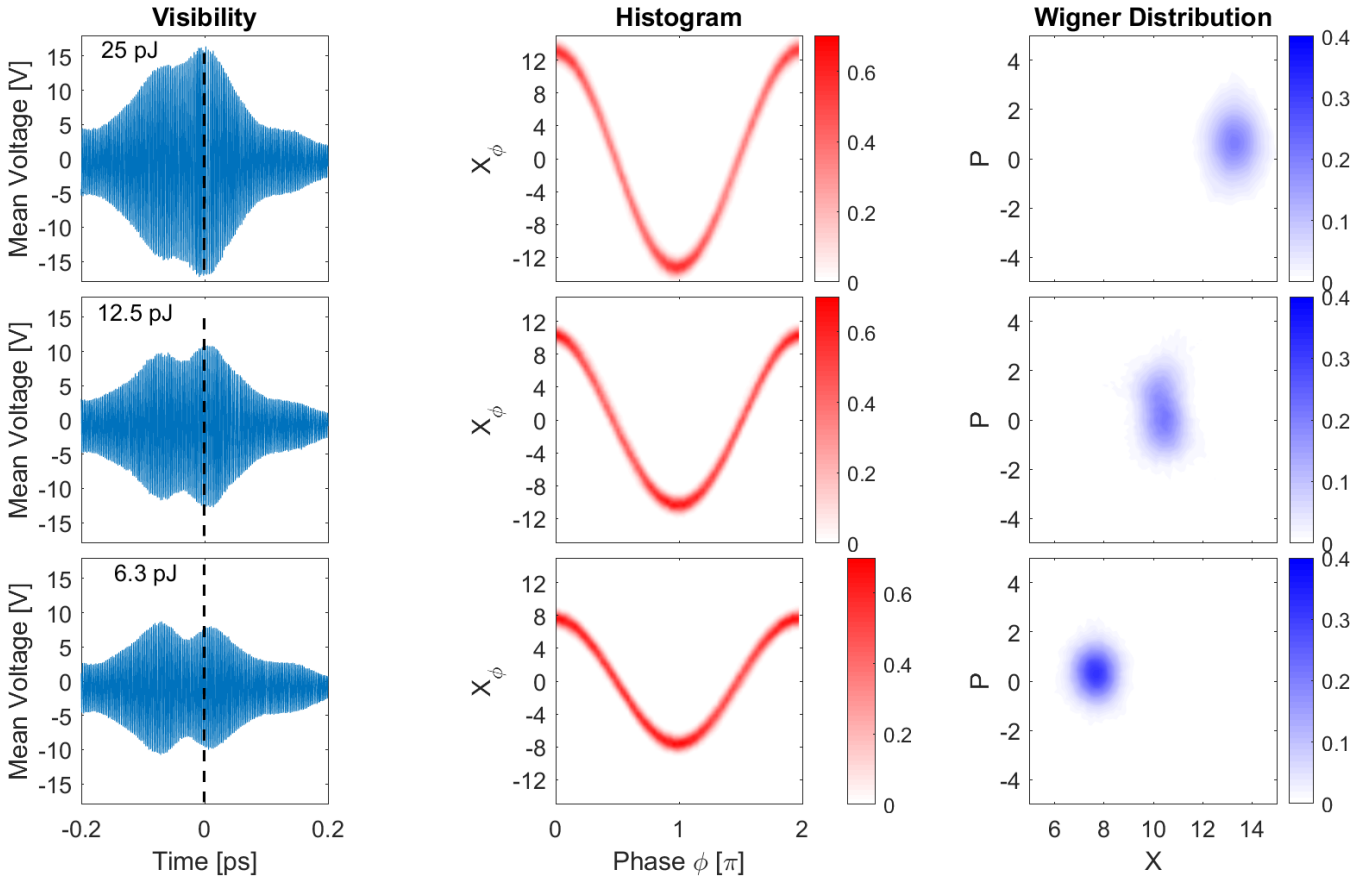


FIG. 2. Measurements of the homodyne system for three different excitation pulse energies. The left column represents the measured temporal correlation between the LO and the signal. The middle column represents the histogram of the normalized output current of the balanced photodetector as a function of the LO phase measured at the vicinity of 0 ps, i.e., the trailing peak, which is indicated by the dashed line in the correlation graph. The right column describes the corresponding Wigner functions. X and P are the quadratures for which $X^2 + P^2 - \frac{1}{2}$ equals the photon number.

the signal at different temporal locations. The center column of Fig. 2 describes histograms of the normalized output current of the balanced photodetector as a function of the LO phase, measured at the trailing peak (dashed line at 0 ps). The corresponding extracted Wigner functions are depicted in the right column, revealing a clear dependence on the input pulse energy. The circular function at 6.3 and the slightly elliptical function at 25 pJ represent displaced thermal states. However, at 12.5 pJ it exhibits a clear elliptical function characteristic of a displaced squeezed thermal state. At any other temporal position, the Wigner functions for all excitation pulse energies exhibit displaced thermal states.

The dependence on pulse excitation energy was examined in detail with the results shown in Fig. 3. The upper left panel shows for reference the circular Wigner distributions of the vacuum and the ASE. Three Wigner functions, measured at 1.56, 6.28, and 9.95 pJ, are basically circular (or are slightly elliptical) describing displaced thermal states. Their distribution is equal to or slightly wider than the standard deviation of the ASE, which is shown in a green circle. The Wigner functions for 3.96 and 15.8 pJ are elliptical. At 3.96 pJ, the system yields a displaced squeezed thermal state. Increasing the input energy by a factor of 4 to 15.8 pJ results in a Wigner function that is squeezed to below the vacuum level (shown as a red circle) in a quadrature close to X.

The experiments were repeated at a range of larger input energies, from 9.95 to 158 pJ, under conditions of somewhat lower input coupling efficiencies to the QD SOA. The results are shown in Fig. 4.

The cyclical nature, with the same fourfold periodicity of the excitation energies, is maintained for 9.95, 35.3, and 125 pJ, yielding elliptical Wigner functions. The narrow axis in those is similar to the standard deviation of the ASE distribution (shown in green circles). Therefore, they do not represent squeezing but rather displaced squeezed thermal states. The higher energies yield multiple Rabi cycles, each contributing a different degree of saturation, and hence, the cumulative effect of the noise modification is less efficient. Moreover, under high excitation energies, nonlinearities such as two-photon absorption modify the saturation properties and hence the nature of the noise modification. The other Wigner functions in the figure describe once more displaced thermal states. Some elliptical Wigner functions in Figs. 3 and 4, in particular, for the higher excitation energies, are tilted. This means that in addition to the obvious relationship between the field amplitude and the phase uncertainties, there exists

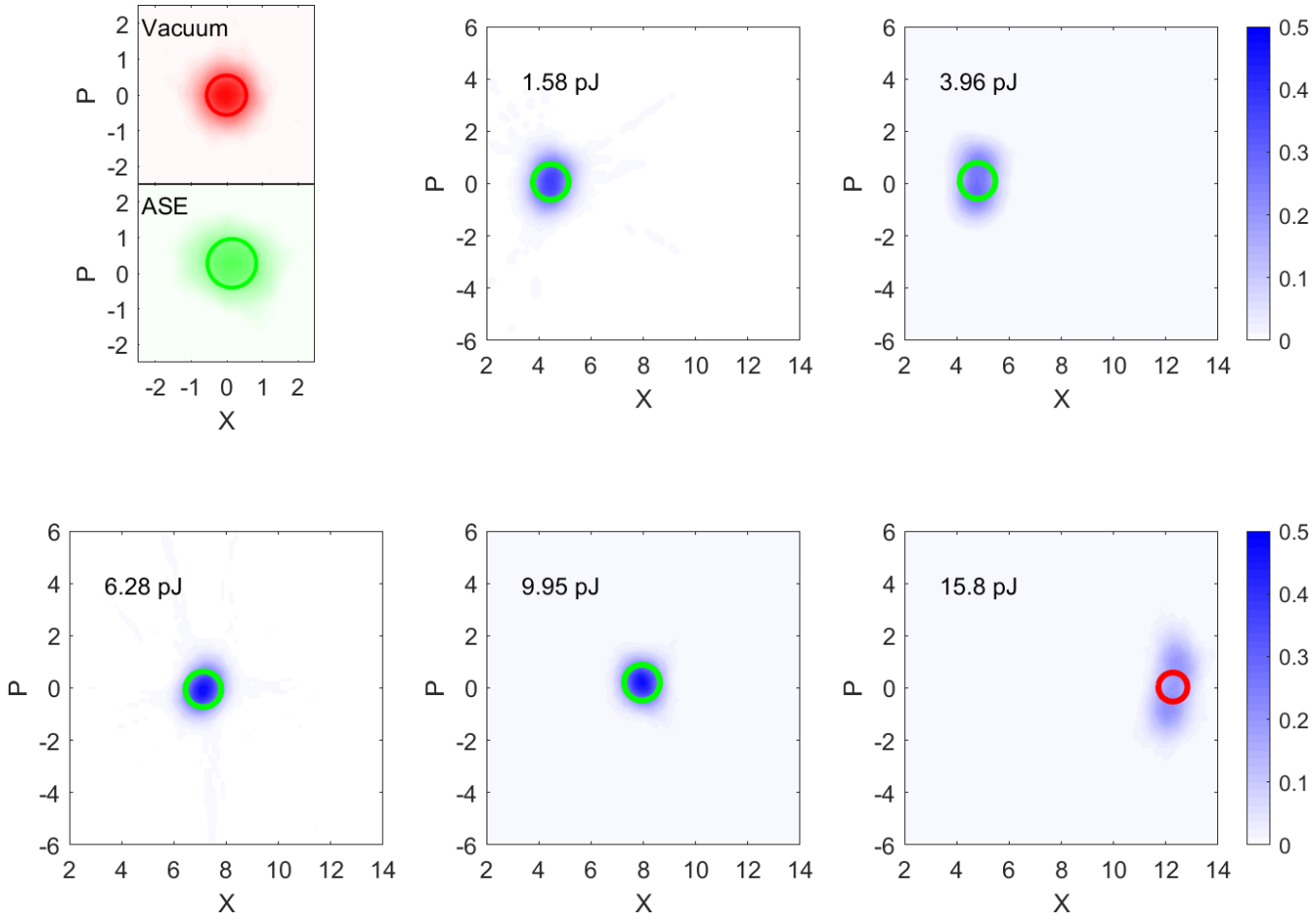


FIG. 3. Excitation-energy-dependent Wigner functions. The upper left panel shows the Wigner distributions of the vacuum (red) and the ASE (green). At 1.56, 6.28, and 9.95 pJ, the Wigner functions are circular. They are equal to or slightly wider than the standard deviation of a Gaussian distribution fit of the Wigner function describing the ASE (green circle), and represent displaced thermal states. The Wigner functions at 3.96 and 15.8 pJ are elliptical. The 3.96 pJ case represents a displaced squeezed thermal state. However, at an excitation energy four times larger, namely, at 15.8 pJ, the state is squeezed in a quadrature close to X.

a nonlinear coupling between them. This is a consequence of the power dependence of the Henry α parameter [41,42].

The cyclical nature of the squeezing is summarized in Fig. 5. The red and blue dots represent the low- and high-energy ranges, respectively. The elliptical Wigner functions are highlighted by circles. Each Wigner distribution was fitted to a two-dimensional (2D) Gaussian distribution with six parameters, and the squeezing ratio shown is the square root of the ratio between the maximum and minimum eigenvalues of the covariance matrix. The parameter fitting errors [43] were propagated to the evaluation of eigenvalues and the squeezing ratio, and the latter's error is denoted by error bars.

The noise properties of the output pulse are clearly cyclical with a periodicity of 4 in the excitation energy or 2π in the pulse area. The physical explanation to this observation stems from the point that the excitation pulse duration (100 fs) is significantly shorter than the room temperature coherence time (about 1 ps) and the dephasing time (roughly 5 ps) of the quantum dots. Such conditions drive the quantum dots into the coherent regime where the pulse area determines the nature of the optically active transition. As the pulse propagates through the gain medium, the quantum dot ensemble is driven through successive cycles of stimulated absorption and stimulated emission, which lead to a periodic dependence of the output field [28]. Noise squeezing occurs only when the system exhibits gain (and gain saturation) and hence the noise accompanying the signal attains the observed cyclical behavior with excitation energy.

In a separate experiment under different operating conditions and coupling losses, a clear squeezed state was observed at an input pulse energy of 25 pJ as seen in Fig. 6(a). Figure 6(b) shows a contour plot of the Wigner (in blue) and vacuum (in red) distributions. The fact that the local oscillator was shot noise limited, as described in Appendix A, ensures that the state is unequivocally squeezed [44].

B. Generation of non-Gaussian state

Under excitation energies of 44.5 and 187 pJ, the obtained Wigner function is non-Gaussian, as seen in Fig. 7. This Wigner function that comprises two bright lobes does not represent any known quantum state. We speculate that it represents a Schrödinger catlike non-Gaussian state. The pulse energies at which the non-Gaussian Wigner function is

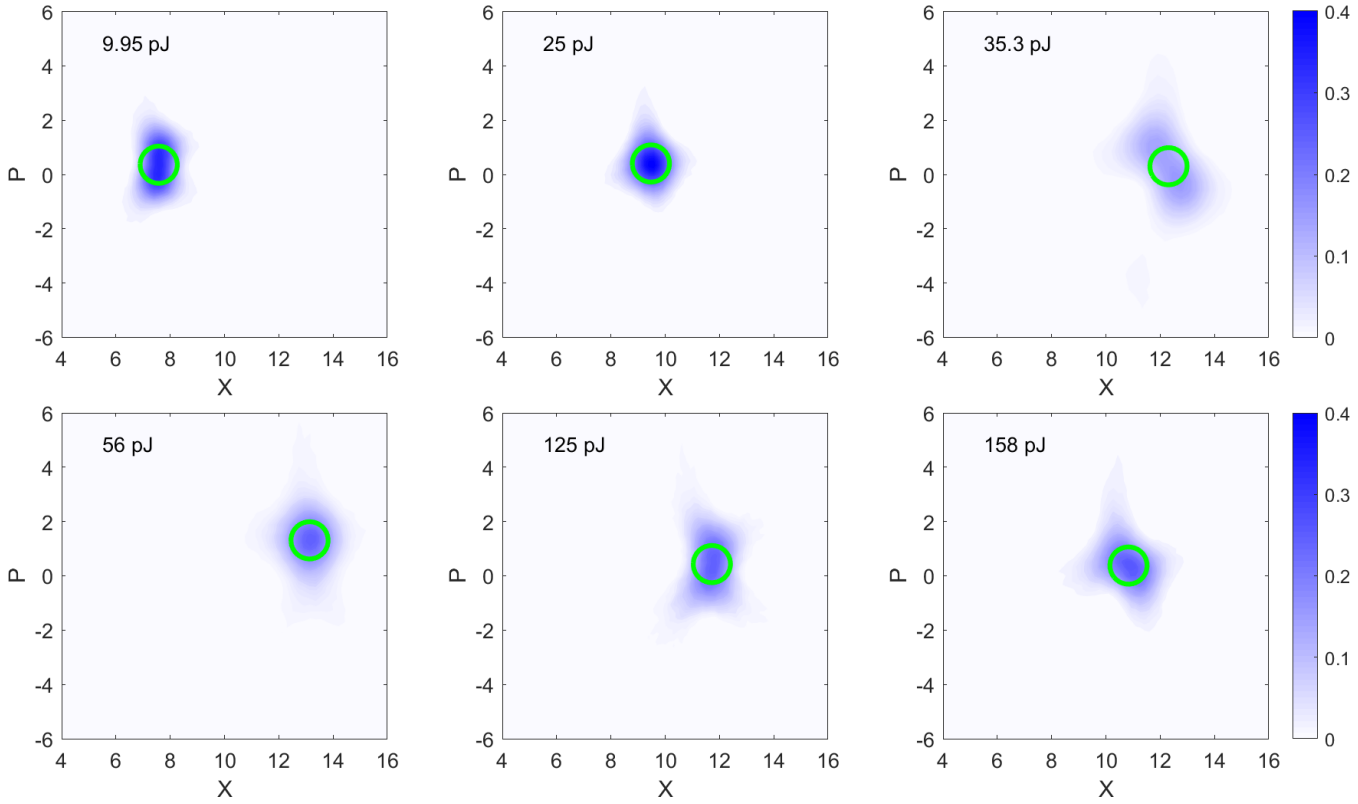


FIG. 4. Wigner functions for large excitation energies. At 9.95, 35.3, and 125 pJ, the Wigner functions are elliptical, while at 25 and 56 pJ they are circular representing displaced thermal states. At 158 pJ, the Wigner function is slightly elliptical. These are equal to or slightly larger than the uncertainty of the ASE, shown as green circles. The elliptical Wigner functions are displaced squeezed thermal states with their narrow axis being similar to the ASE shown in green circles.

observed correspond to pulse areas equal to an integer number n of full Rabi cycles, followed by an additional quarter-cycle rotation on the Bloch sphere, namely, $2\pi n + \pi/2$. These non-Gaussian states also repeat for every fourfold increase in excitation energy.

In the assumed Schrödinger catlike non-Gaussian state, the negative regime is omitted. We speculate that this omission is due to large output losses. We emphasize that this is a speculation that is not proven unequivocally. However, a simulation that assumed a Schrödinger cat state that undergoes a 10 dB loss strongly suppresses the interference fringes while preserving the bimodal phase-space structure finally yielding a Wigner function similar to the measured one, as described in Fig. 7. The non-Gaussian Wigner function is observed when the quantum dot gain medium is biased to transparency. Under those conditions, the quantum dots are prepared in a coherent superposition of optical coherent states corresponding to the matter's ground and excited states. This leads to competing gain and absorption processes. A final transparent state collapses then into two distinct dynamical trajectories on the Bloch sphere during the driven evolution, giving rise to quantum interference between these pathways. This interference manifests itself in phase space as a split Wigner function, which in the absence of loss is expected to exhibit oscillatory fringes and Wigner negativity signifying quantum interference.

Observation of Wigner negativity requires that optical losses are smaller than 50%. In the present experiment, the

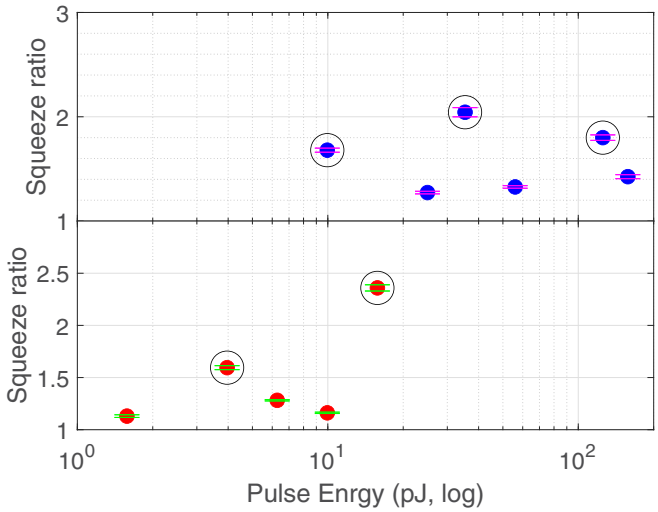


FIG. 5. Squeezing level as a function of excitation pulse energy for the two energy domains. The red dots correspond to Fig. 3, while the blue dots describe the data from Fig. 4. Each Wigner distribution was fitted to a 2D Gaussian distribution, and the squeezing ratio shown is the square root of the ratio between the maximum and minimum eigenvalues of the covariance matrix. The points representing elliptical Wigner functions are highlighted by circles. Parameter fitting errors are marked by error bars. Note that in all cases, the error bars are rather small.

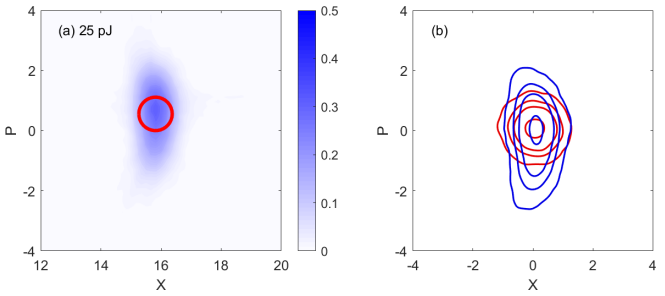


FIG. 6. Squeezed state at an excitation of 25 pJ. (a) Squeezed Wigner function distribution. The red circle represents the vacuum. (b) Contour plots of the Wigner distributions of vacuum and displaced squeezed states. The full width at half maximum in the X axis is reduced from 1.43 for the vacuum state to 1.17 for the squeezed state. This corresponds to approximately 1.5 dB of quadrature-noise reduction relative to the vacuum reference.

output losses that result from inefficient collection at the gain medium output, propagation losses, mode-matching losses, filtering losses, and detection inefficiencies are large, close to 10 dB, and hence, the negativity cannot be observed [38,45,46].

The measured non-Gaussian states are shown in Figs. 7(a) and 7(b). The non-Gaussian function we assume is shown in Fig. 7(c). The calculated evolution of this state due to the output optical loss yields the Wigner function shown in Fig. 7(d), which is consistent with the measured functions. The details of the calculation are presented in Appendix B.

III. DISCUSSION

In this work, we demonstrated a direct interplay between Rabi oscillations in a room-temperature QD SOA, induced by an ultrashort excitation pulse and noise. Specifically, Rabi oscillations cause cyclical modifications of the output field amplitude uncertainty. This effect repeats with every fourfold increase in the excitation pulse energy, equivalent to a 2π increment in pulse area amounting to a full cycle on the Bloch sphere. The noise in those cases takes on a value that is similar to or slightly smaller than the standard deviation of the ASE level of a linear amplifier. In some cases, it is actually squeezed to below the vacuum level. This behavior was observed for 2 orders of magnitude range of excitation energies. Naturally, the conjugate phase quadrature noise increases correspondingly.

The underlying mechanism of the cyclical noise modification arises from the periodic evolution between gain and absorption in the QD SOA during Rabi oscillations. The field amplitude uncertainty is reduced during portions of the Rabi cycle when the QDs provide gain saturation; otherwise, the output exhibits the noise properties of a displaced thermal state. However, there are some specific excitation levels that yield very unique results. A clear squeezed state and a non-Gaussian Wigner function were demonstrated.

The latter resembles a Schrödinger catlike non-Gaussian state where the negativity is omitted, possibly due to a large optical loss between the SOA output facet and the homodyne system. Simulations including the measured optical loss show

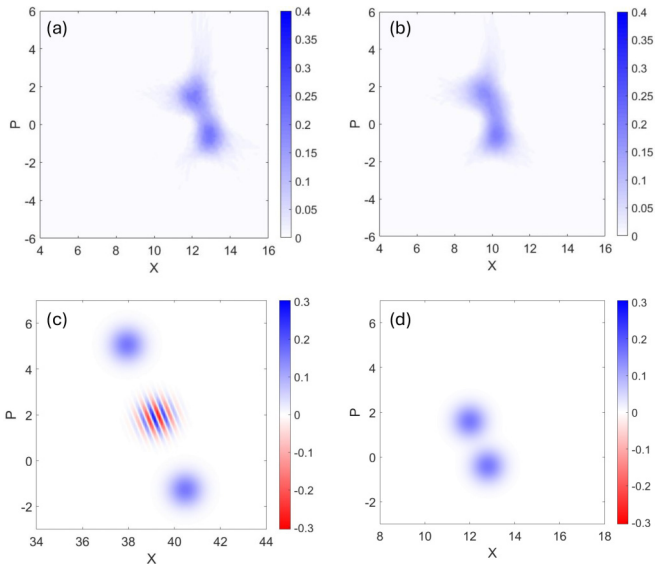


FIG. 7. Non-Gaussian Wigner functions measured at (a) 44.5 pJ and (b) 187 pJ (a fourfold increase). This Wigner function does not represent any known quantum state. However, it resembles a Schrödinger catlike non-Gaussian state except that the negativity between the two bright lobes is absent, possibly due to the system optical losses of 10 dB. (c) Simulated Wigner functions of the cat state $\frac{|37.9+5i\rangle+|40.5-1.3i\rangle}{\mathcal{N}}$ (where $\mathcal{N}$ is a normalization factor) and (d) the reconstructed state after undergoing 10 dB of coupling loss.

that such loss would strongly suppress the interference fringes while preserving the bimodal phase-space structure.

Our findings represent a clear manipulation of noise (amplifier added ASE and noise carried by the input signal) via coherent light-matter interactions. This is a fundamentally new regime of amplifier operation that could enable engineered noise profiles in active photonic devices. Potential applications include tailored noise suppression in optical amplifiers for quantum communication systems or enhanced sensitivity in measurement schemes where reduced amplitude noise is crucial.

Future research should explore this effect in cavity-based systems with tailored feedback. Additionally, incorporating pulse shaping techniques to precisely control and optimize the temporal dynamics of the Rabi oscillations [47] may enhance the noise reduction while opening new avenues for deterministic quantum noise engineering on chip-scale photonic platforms.

ACKNOWLEDGMENTS

The research was partially supported by the Israel Science Foundation under Grant No. 1487/26 and by the Hellen Diller Quantum Center at Technion. We thank Prof. Maria Chekhova for her insightful suggestions and support throughout this project. This research was supported by a scholarship sponsored by the Ministry of Innovation, Science and Technology, Israel.

DATA AVAILABILITY

There are no publicly available research data or software supporting this manuscript. Requests for further information or data should be sent to the authors.

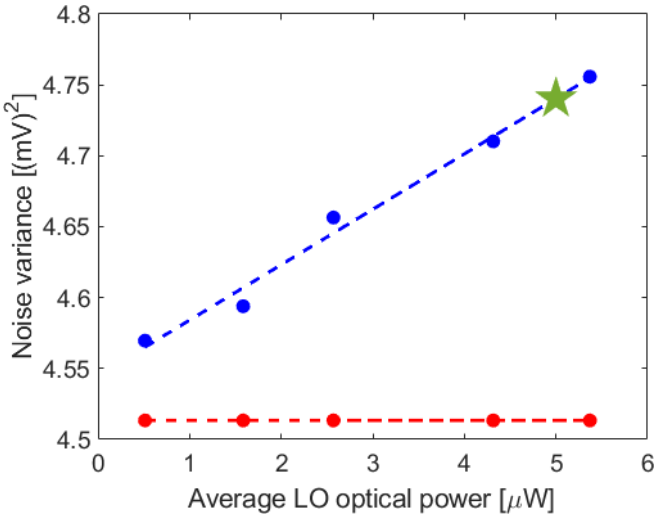


FIG. 8. The blue trace represents the measured shot noise variance of the LO as a function of its average power feeding the balance detector system. The green star represents the power under which the experiments were performed. Since it is within the linear regime, the LO was indeed shot noise limited. The red trace represents the background electrical noise of the system.

APPENDIX A: SHOT NOISE MEASUREMENT

The measurements of squeezed states, described in Figs. 3 and 4, rely on the fact that the LO is shot noise limited. To this end, we have measured the noise variance of the LO as a function of its average power. The results are shown in Fig. 8. The average LO power used in the experiments was 5 μW (marked by a green star). This power is within the linear range of the curve proving that the LO was indeed shot noise limited.

APPENDIX B: LOSS INFLUENCE ON QUANTUM STATES

A conventional model for optical loss is a beam splitter (BS) with a reflection coefficient $\sqrt{L} \triangleq \sin(\theta)$, where L is the coupling loss. A general BS with two input modes and two output modes is represented as follows:

$$\begin{pmatrix}\hat{b}_1\\ \hat{b}_2\end{pmatrix} = \begin{pmatrix}\cos(\theta) & ie^{i\phi}\sin(\theta)\\ ie^{-i\phi}\sin(\theta) & \cos(\theta)\end{pmatrix}\begin{pmatrix}\hat{a}_1\\ \hat{a}_2\end{pmatrix}, \tag{B1}$$

where $\hat{a}_1, \hat{a}_2$ are the annihilation operators of the input modes and $\hat{b}_1, \hat{b}_2$ are the annihilation operators of the output modes.

The annihilation operator $\hat{a}$ and its conjugate creation operator $\hat{a}^\dagger$ satisfy the standard relations:

$$\hat{a}|n\rangle = \sqrt{n}|n-1\rangle, \tag{B2}$$

$$\hat{a}^\dagger|n\rangle = \sqrt{n+1}|n+1\rangle. \tag{B3}$$

One can set the phase $\phi = 0$ and write the inverse of the BS matrix:

$$\begin{pmatrix}\hat{a}_1\\ \hat{a}_2\end{pmatrix} = \begin{pmatrix}\cos(\theta) & -i\sin(\theta)\\ -i\sin(\theta) & \cos(\theta)\end{pmatrix}\begin{pmatrix}\hat{b}_1\\ \hat{b}_2\end{pmatrix}. \tag{B4}$$

Consequently, the input annihilation operators are expressed in terms of the output operators as

$$\hat{a}_1 = \cos(\theta)\hat{b}_1 - i\sin(\theta)\hat{b}_2, \tag{B5}$$

$$\hat{a}_2 = -i\sin(\theta)\hat{b}_1 + \cos(\theta)\hat{b}_2. \tag{B6}$$

Consider an initial state consisting of a Fock state $|n\rangle$ in input mode 1 ($\rho_{\text{init}} = |n\rangle\langle n|$) and the vacuum state in input mode 2. Under the BS operation, the state evolves according to Eq. (B5):

$$|n,0\rangle = \frac{(\hat{a}_1^\dagger)^n}{\sqrt{n!}}|0,0\rangle$$

$$\rightarrow |\Psi_{\text{BS}}\rangle = \frac{(\cos(\theta)\hat{b}_1^\dagger + i\sin(\theta)\hat{b}_2^\dagger)^n}{\sqrt{n!}}|0,0\rangle. \tag{B7}$$

Using Eq. (B3) and applying the binomial expansion, one can show that the output state is given by

$$|\Psi_{\text{BS}}\rangle = \sum_{m=0}^{n}\sqrt{\binom{n}{m}}\cos^m(\theta)i^{n-m}\sin^{n-m}(\theta)|m, n-m\rangle. \tag{B8}$$

The corresponding density matrix is

$$\rho_{\text{BS}} = \sum_{m=0}^{n}\sum_{k=0}^{n}\sqrt{\binom{n}{m}\binom{n}{k}}\cos^{m+k}(\theta)(-1)^{n-k}i^{2n-m-k} \times \sin^{n-m}(\theta)|m, n-m\rangle\langle k, n-k|. \tag{B9}$$

To determine the state in port 1 after experiencing an output loss, we perform a partial trace over the second mode:

$$\rho_{\text{final}} = \sum_{m=0}^{n}\binom{n}{m}\cos^{2m}(\theta)\sin^{2(n-m)}(\theta)|m\rangle\langle m|$$

$$= \sum_{m=0}^{n}\binom{n}{m}(1-L)^m L^{n-m}|m\rangle\langle m|. \tag{B10}$$

This resulting density matrix is diagonal in the Fock basis.

Equation (B10) characterizes the action of the amplitude damping channel $\mathcal{E}_{\text{amp}}$ on an initial Fock state $|n\rangle\langle n|$. The probability of losing exactly k photons is

$$P_{n\rightarrow n-k} = \text{Tr}(\rho_{\text{final}}|n-k\rangle\langle n-k|)$$

$$= \binom{n}{n-k}(1-L)^{n-k}L^k. \tag{B11}$$

To represent this channel via its Kraus decomposition, we define the Kraus operators $\hat{M}_k$. These operators possess nonzero elements only on their kth superdiagonal, representing transitions from $|n\rangle$ to $|n-k\rangle$:

$$P_{n\rightarrow n-k} = \text{Tr}(\rho_{\text{final}}|n-k\rangle\langle n-k|)$$

$$= \text{Tr}\left(\sum_{m=0}^{N}\hat{M}_m\rho_{\text{init}}\hat{M}_m^\dagger|n-k\rangle\langle n-k|\right)$$

$$= \sum_{m=0}^{N}\langle n-k|\hat{M}_m|n\rangle\langle n|M_m^\dagger|n-k\rangle$$

$$= |\langle n-k|\hat{M}_k|n\rangle|^2, \tag{B12}$$

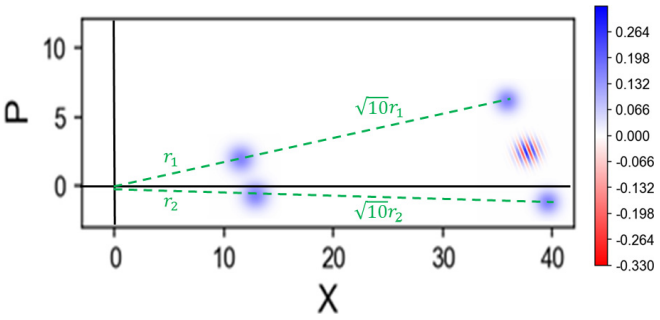


FIG. 9. Phase-space representation of the state evolution under coupling loss. Wigner functions of the initial cat state $\frac{|37.9+5i\rangle+|40.5-1.3i\rangle}{\mathcal{N}}$ (where $\mathcal{N}$ is a normalization factor) before dissipative influence (right) and the reconstructed state after undergoing 10 dB of coupling loss (left). A 10 dB loss results in a $\sqrt{10}$ attenuation of the amplitude for each coherent component, leading to suppression of the quantum interference pattern. Yet, the angular orientation of the peaks in phase space remains invariant under this dissipative process.

where $N+1$ is the Hilbert space dimension, and in a Kraus map, the following occurs:

$$\rho_{\text{final}} = \sum_{n=0}^{N} \hat{M}_n \rho_{\text{init}} \hat{M}_n^\dagger, \quad \mathbb{I} = \sum_{n=0}^{N} \hat{M}_n^\dagger \hat{M}_n. \tag{B13}$$

From this relation, the matrix elements are determined up to a phase:

$$\langle n-k|\hat{M}_k|n\rangle = \sqrt{P_{n\to n-k}}\, e^{i\varphi_{n\to n-k}} = \sqrt{\binom{n}{n-k}(1-L)^{n-k}L^k}\, e^{i\varphi_{n\to n-k}}. \tag{B14}$$

This phase may be neglected, as it acts as a global phase during the mapping of the density matrix. The Kraus operator is thus written as

$$\hat{M}_k = \sum_{n=k}^{N} \sqrt{\binom{n}{n-k}(1-L)^{n-k}L^k}\, |n-k\rangle\langle n|. \tag{B15}$$

Note that in the limit of total loss ($L=1$), the initial state is mapped entirely to the vacuum state, such that

$$\hat{M}_k(L=1) = |0\rangle\langle k|. \tag{B16}$$

The negativity of the original quantum state is diminished when the loss exceeds 3 dB [46]. The Kraus operators defined in Eqs. (B15) and (B16) were implemented in a Python-based simulation to model the dissipative dynamics of the system. Figure 9 displays the results of this simulation, comparing the initial cat state with its representation after undergoing 10 dB of coupling loss.

[1] C. M. Caves, Quantum-mechanical noise in an interferometer, Phys. Rev. D **23**, 1693 (1981).

[2] R. E. Slusher, L. W. Hollberg, B. Yurke, J. C. Mertz, and J. F. Valley, Observation of squeezed states generated by four-wave mixing in an optical cavity, Phys. Rev. Lett. **55**, 2409 (1985).

[3] U. L. Andersen, T. Gehring, C. Marquardt, and G. Leuchs, 30 years of squeezed light generation, Phys. Scr. **91**, 053001 (2016).

[4] J. Aasi, J. Abadie, B. P. Abbott, R. Abbott, T. D. Abbott, M. R. Abernathy, C. Adams, T. Adams, P. Addesso, R. X. Adhikari, *et al.*, Enhanced sensitivity of the LIGO gravitational wave detector by using squeezed states of light, Nat. Photon. **7**, 613 (2013).

[5] R. E. Slusher and B. Yurke, Squeezed light for coherent communications, J. Lightwave Technol. **8**, 466 (2002).

[6] H. P. Yuen, *Communication and Measurement with Squeezed States* (Springer-Verlag, Berlin, Heidelberg GmbH, 2004), pp. 227–261.

[7] I. Suleiman, J. A. H. Nielsen, X. Guo, N. Jain, J. Neergaard-Nielsen, T. Gehring, and U. L. Andersen, 40 km fiber transmission of squeezed light measured with a real local oscillator, Quantum Sci. Technol. **7**, 045003 (2022).

[8] U. L. Andersen, J. S. Neergaard-Nielsen, P. van Loock, and A. Furusawa, Hybrid discrete- and continuous-variable quantum information, Nat. Phys. **11**, 713 (2015).

[9] S. Takeda and A. Furusawa, Toward large-scale fault-tolerant universal photonic quantum computing, APL Photon. **4**, 060902 (2019).

[10] R. W. Boyd, A. L. Gaeta, and E. Giese, *Nonlinear Optics* (Elsevier, Burlington, 2008), pp. 22–31.

[11] L.-A. Wu, H. Kimble, J. Hall, and H. Wu, Generation of squeezed states by parametric down conversion, Phys. Rev. Lett. **57**, 2520 (1986).

[12] C. McCormick, V. Boyer, E. Arimondo, and P. Lett, Strong relative intensity squeezing by four-wave mixing in rubidium vapor, Opt. Lett. **32**, 178 (2007).

[13] J. Heersink, V. Josse, G. Leuchs, and U. L. Andersen, Efficient polarization squeezing in optical fibers, Opt. Lett. **30**, 1192 (2005).

[14] K. Bergman and H. Haus, Squeezing in fibers with optical pulses, Opt. Lett. **16**, 663 (1991).

[15] A. Bilenca and G. Eisenstein, On the noise properties of linear and nonlinear quantum-dot semiconductor optical amplifiers: The impact of inhomogeneously broadened gain and fast carrier dynamics, IEEE J. Quantum Electron. **40**, 690 (2004).

[16] T. W. Berg and J. Mork, Saturation and noise properties of quantum-dot optical amplifiers, IEEE J. Quantum Electron. **40**, 1527 (2004).

[17] A. Bogoni, L. Poti, C. Porzi, M. Scaffardi, P. Ghelfi, and F. Ponzini, Modeling and measurement of noisy SOA dynamics for ultrafast applications, IEEE J. Sel. Top. Quantum Electron. **10**, 197 (2004).

[18] Y. Yamamoto, S. Machida, and W. H. Richardson, Photon number squeezed states in semiconductor lasers, Science **255**, 1219 (1992).

[19] S. Machida, Y. Yamamoto, and Y. Itaya, Observation of amplitude squeezing in a constant-current–driven semiconductor laser, Phys. Rev. Lett. **58**, 1000 (1987).

[20] J. Kitching, A. Yariv, and Y. Shevy, Room temperature generation of amplitude squeezed light from a semiconductor laser with weak optical feedback, Phys. Rev. Lett. **74**, 3372 (1995).

[21] S. Zhao, S. Ding, H. Huang, I. Zaquine, N. Fabre, N. Belabas, and F. Grillot, Broadband amplitude squeezing at room temperature in electrically driven quantum dot lasers, Phys. Rev. Res. **6**, L032021 (2024).

[22] J.-L. Vey and P. Gallion, Semiclassical model of semiconductor laser noise and amplitude noise squeezing. I. Description and application to Fabry-Perot laser, IEEE J. Quantum Electron. **33**, 2097 (1997).

[23] M. Shtaif and G. Eisenstein, Noise properties of nonlinear semiconductor optical amplifiers, Opt. Lett. **21**, 1851 (1996).

[24] A. Capua, V. Mikhelashvili, G. Eisenstein, J. Reithmaier, A. Somers, A. Forchel, M. Calligaro, O. Parillaud, and M. Krakowski, Direct observation of the coherent spectral hole in the noise spectrum of a saturated InAs/InP quantum dash amplifier operating near 1550 nm, Opt. Express **16**, 2141 (2008).

[25] M. Shtaif and G. Eisenstein, Experimental study of the statistical properties of nonlinearly amplified signals in semiconductor optical amplifiers, IEEE Photonics Technol. Lett. **9**, 904 (2002).

[26] A. Bilenca and G. Eisenstein, Statistical noise properties of an optical pulse propagating in a nonlinear semiconductor optical amplifier, IEEE J. Quantum Electron. **41**, 36 (2005).

[27] A. Bilenca and G. Eisenstein, Fokker–Planck and Langevin analyses of noise accompanying the amplification of optical pulses in semiconductor optical amplifiers, J. Opt. Soc. Am. B **22**, 1632 (2005).

[28] G. Eisenstein, J. P. Reithmaier, A. Capua, O. Karni, A. K. Mishra, S. Bauer, and I. Khanonkin, Coherent light matter interactions in nanostructure based active semiconductor waveguides operating at room temperature, Appl. Phys. Rev. **6**, 041317 (2019).

[29] I. Khanonkin, O. Eyal, J. P. Reithmaier, and G. Eisenstein, Room-temperature coherent revival in an ensemble of quantum dots, Phys. Rev. Res. **3**, 033073 (2021).

[30] A. Capua, O. Karni, G. Eisenstein, and J. P. Reithmaier, Rabi oscillations in a room-temperature quantum dash semiconductor optical amplifier, Phys. Rev. B **90**, 045305 (2014).

[31] P. Borri, W. Langbein, S. Schneider, U. Woggon, R. Sellin, D. Ouyang, and D. Bimberg, Coherent light–matter interaction in InGaAs quantum dots: Dephasing time and optical Rabi oscillations, Phys. Status Solidi B **233**, 391 (2002).

[32] M. Kolarczik, N. Owschimikow, J. Korn, B. Lingnau, Y. Kaptan, D. Bimberg, E. Schöll, K. Lüdge, and U. Woggon, Quantum coherence induces pulse shape modification in a semiconductor optical amplifier at room temperature, Nat. Commun. **4**, 2953 (2013).

[33] H. Choi, V.-M. Gkortsas, L. Diehl, D. Bour, S. Corzine, J. Zhu, G. Höfler, F. Capasso, F. X. Kärtner, and T. B. Norris, Ultrafast Rabi flopping and coherent pulse propagation in a quantum cascade laser, Nat. Photon. **4**, 706 (2010).

[34] J.-Z. Zhang and I. Galbraith, Rabi oscillations of ultrashort optical pulses in 1.55 μm InGaAs/InGaAsP quantum-well amplifiers, J. Appl. Phys. **96**, 922 (2004).

[35] E. Wigner, On the quantum correction for thermodynamic equilibrium, Phys. Rev. **40**, 749 (1932).

[36] M. S. Kim, F. A. M. de Oliveira, and P. L. Knight, Properties of squeezed number states and squeezed thermal states, Phys. Rev. A **40**, 2494 (1989).

[37] H. Jeong and T. C. Ralph, Transfer of nonclassical properties from a microscopic superposition to macroscopic thermal states in the high temperature limit, Phys. Rev. Lett. **97**, 100401 (2006).

[38] M. Cosacchi, T. Seidelmann, J. Wiercinski, M. Cygorek, A. Vagov, D. E. Reiter, and V. M. Axt, Schrödinger cat states in quantum-dot-cavity systems, Phys. Rev. Res. **3**, 023088 (2021).

[39] S. Banyoudeh and J. P. Reithmaier, High-density 1.54 μm InAs/InGaAlAs/InP (100) based quantum dots with reduced size inhomogeneity, J. Cryst. Growth **425**, 299 (2015).

[40] S. R. Deans, *The Radon Transform and Some of Its Applications* (Dover Publication Inc, Mineola, 2007).

[41] T. Septon, A. Becker, S. Gosh, G. Shtendel, V. Sichkovskyi, F. Schnabel, A. Sengül, M. Bjelica, B. Witzigmann, J. P. Reithmaier, and G. Eisenstein, Large linewidth reduction in semiconductor lasers based on atom-like gain material, Optica **6**, 1071 (2019).

[42] M. Bjelica and B. Witzigmann, Optimization of 1.55 μm quantum dot edge-emitting lasers for narrow spectral linewidth, Opt. Quantum Electron. **48**, 110 (2016).

[43] W. H. Press, S. A. Teukolsky, W. T. Vetterling, and B. P. Flannery, *Numerical Recipes: The Art of Scientific Computing*, 3rd ed. (Cambridge University Press, Cambridge, UK, 2007).

[44] H. Vahlbruch, M. Mehmet, S. Chelkowski, B. Hage, A. Franzen, N. Lastzka, S. Goßler, K. Danzmann, and R. Schnabel, Observation of squeezed light with 10-dB quantum-noise reduction, Phys. Rev. Lett. **100**, 033602 (2008).

[45] A. I. Lvovsky and M. G. Raymer, Continuous-variable optical quantum-state tomography, Rev. Mod. Phys. **81**, 299 (2009).

[46] A. I. Lvovsky and J. H. Shapiro, Nonclassical character of statistical mixtures of the single-photon and vacuum optical states, Phys. Rev. A **65**, 033830 (2002).

[47] O. Karni, A. K. Mishra, G. Eisenstein, V. Ivanov, and J. P. Reithmaier, Coherent control in room-temperature quantum dot semiconductor optical amplifiers using shaped pulses, Optica **3**, 570 (2016).